



**HAL**  
open science

# Origin of the Annual to Decadal Peaks of Variability in the Response of Simple Ocean Models to Stochastic Forcing

Jérôme Sirven, Christophe Herbaut, Julie Deshayes, Claude Frankignoul

► **To cite this version:**

Jérôme Sirven, Christophe Herbaut, Julie Deshayes, Claude Frankignoul. Origin of the Annual to Decadal Peaks of Variability in the Response of Simple Ocean Models to Stochastic Forcing. *Journal of Physical Oceanography*, 2007, 37, pp.2146. 10.1175/JPO3095.1 . hal-00770700

**HAL Id: hal-00770700**

**<https://hal.science/hal-00770700>**

Submitted on 10 Jun 2021

**HAL** is a multi-disciplinary open access archive for the deposit and dissemination of scientific research documents, whether they are published or not. The documents may come from teaching and research institutions in France or abroad, or from public or private research centers.

L'archive ouverte pluridisciplinaire **HAL**, est destinée au dépôt et à la diffusion de documents scientifiques de niveau recherche, publiés ou non, émanant des établissements d'enseignement et de recherche français ou étrangers, des laboratoires publics ou privés.

## Origin of the Annual to Decadal Peaks of Variability in the Response of Simple Ocean Models to Stochastic Forcing

JÉRÔME SIRVEN, CHRISTOPHE HERBAUT, JULIE DESHAYES, AND CLAUDE FRANKIGNOUL

*LOCEAN/IPSL, Université Pierre et Marie Curie, Paris, France*

(Manuscript received 11 April 2006, in final form 18 October 2006)

### ABSTRACT

The response of the ocean to stochastic forcings is studied in a closed basin, using a simple one-dimensional analytical model. The focus is on the mechanisms that determine the time scales of the response and their possible links with free basin modes. The response may be described as a forced solution plus propagating solutions whose spatial pattern does not depend on the forcing. The propagating solutions are of two types. The first ones propagate eastward and are strongly damped so that their influence remains limited to the western boundary layer. The others are damped long Rossby waves that propagate westward and whose amplitude depends on the spatial extension and the frequency of the forcing. The amplitude increases if the frequency of the forcing is close to the frequency of the basin modes, but the spatial pattern differs from that of the latter; higher frequencies are favored if the zonal extension of the forcing is reduced. The response of a 1.5-layer reduced-gravity ocean model forced by stochastic Ekman pumping confirms the results of the analytical model.

### 1. Introduction

There is increasing evidence that the decadal variability of the midlatitude ocean (e.g., Kushnir 1994; Deser et al. 1999) primarily reflects the variability of the atmosphere via stochastic wind stress forcing. Considering a stratified model with an open western boundary, Frankignoul et al. (1997) found that the oceanic response was largest at decadal frequency, but no spectral peak appeared (see also Sirven et al. 2002). LaCasce (2000) and Cessi and Louazel (2001) considered the ocean response in a closed basin and found that decadal peaks may appear because of the global mass conservation constraint. They suggested that the peaks were associated with the existence of free basin modes, as their period was very close to the period of the least damped modes. Cessi and Otheguy (2003) showed that wind stress forcing in the Northern Hemisphere could excite a substantial response in the Southern Hemisphere, whose pattern was very similar to that of the least-damped basin mode. The mechanism explaining the existence of the free basin modes is simple: long

Rossby waves propagate westward to the western boundary. Along the latter, the energy is transmitted equatorward then eastward, where it is radiated again westward by long Rossby waves. For the connection between the western and the eastern boundary, Wajsowicz and Gill (1986) and Milliff and McWilliams (1994) suggested a coupling between rapid coastal Kelvin waves, generated by the mass adjustment process, and slower baroclinic Rossby waves. Primeau (2002) suggested, instead, that the Rossby waves force low frequency, large-scale gravity waves that enforce mass conservation and carry the energy back to the eastern boundary.

The characteristics of the free basin modes are robust in shallow-water and quasigeostrophic models. Primeau (2002) showed that the ability of these modes to be resonantly excited depends on the efficiency with which energy is transmitted from the western boundary back to the eastern boundary: this efficiency is greatly reduced when the basin-crossing time of long Rossby waves is latitude dependent. Cessi and Louazel (2001) and Primeau (2002) suggested that the decay rate of the basin modes is independent of the friction to leading order, and LaCasce and Pedlosky (2002) showed that the emergence of the long-wave free modes requires sufficiently large friction. They also found that forced solutions that *resemble* the long-wave modes may be

---

*Corresponding author address:* Dr. Jérôme Sirven, LOCEAN/IPSL, Université Pierre et Marie Curie, Tour 45, étage 4, CC100, 4 Place Jussieu, 75252 Paris CEDEX 05, France.  
E-mail: js@lodyc.jussieu.fr

seen even if the large friction requirement is not fulfilled. Lastly, LaCasce and Pedlosky (2004) proved that Rossby basin modes may become baroclinically unstable if the transit time of the long Rossby waves becomes larger than the  $e$ -folding time associated with the instability.

Linear models that conserve the total mass were also used to study the response to fluctuations in the volume transport across the northern boundary, which might reflect changes in deep-water formation (Johnson and Marshall 2002, 2004; Deshayes and Frankignoul 2005). Although the models were similar to that of Cessi and Louazel (2001) and therefore included the basin modes, no spectral peaks were found at decadal time scale except in the vicinity of the northern boundary.

Considering these contrasting results, it is worth investigating further whether free basin modes can be efficiently excited. In this paper, we consider a simple analytical model of a closed ocean basin, whose complexity is halfway between that of the models of Frankignoul et al. (1997) and Cessi and Louazel (2001). The model is stochastically forced by a standing spatial pattern, and the emphasis is on the mechanisms that determine the dominant time scales of the response (section 2). We then investigate to what extent the results are robust in a more realistic context, using a nonlinear 1.5-layer reduced-gravity model forced by stochastic Ekman pumping (section 3). Conclusions are given in section 4.

## 2. A one-dimensional model of a midlatitude ocean

### a. Description of the model

For a rectangular basin  $\mathcal{D}$  in the  $\beta$  plane, the governing equations of a linearized reduced-gravity 1.5-layer model are

$$\partial_t u - fv = -g' \partial_x h - \epsilon u + \tau/(\rho_1 \mathcal{H}), \quad (1)$$

$$\partial_t v + fu = -g' \partial_y h - \epsilon v, \quad \text{and} \quad (2)$$

$$\partial_t h + \mathcal{H}(\partial_x u + \partial_y v) = -\lambda h + \mathcal{S}, \quad (3)$$

where  $u$ ,  $v$ , and  $h$  are, respectively, the zonal velocity, the meridional velocity, and the interface displacement (positive upward),  $\rho_1$  is the density of the upper layer and  $\mathcal{H}$  is its mean thickness,  $g'$  is the reduced gravity,  $f = f_0 + \beta y$  is the Coriolis parameter,  $\epsilon$  is a constant drag coefficient, and  $\tau(y, t)$  is the wind stress, assumed for simplicity to be zonal and independent of longitude. The term  $-\lambda h$  parameterizes the vertical diffusivity by a Newtonian damping (Huang et al. 2000), and  $\mathcal{S}$  represents the external sources or sinks of mass (e.g., due

to deep convection). As there is no normal flow along the boundaries, the mass conservation Eq. (3) yields

$$\frac{d}{dt} \iint_{\mathcal{D}} h \, dx \, dy = \iint_{\mathcal{D}} (\mathcal{S} - \lambda h) \, dx \, dy = 0,$$

if the water volume  $\iint_{\mathcal{D}} h \, dx \, dy$  remains constant—that is, if there is an exact balance between the sources and sinks of mass.

We assume for simplicity that the coastal Kelvin waves are infinitely fast, or equivalently that the terms  $\partial_t u$  and  $\partial_t v$  can be neglected in Eqs. (1) and (2). We thus only consider the slower propagation of the long Rossby waves across the basin. The variations of the interface are then given by

$$\partial_t h - c \partial_x h + \frac{2\epsilon}{f} \partial_y h = w_e - \lambda h + \mathcal{S} + \frac{g' \epsilon}{f^2} \Delta h, \quad (4)$$

where  $c = \beta g' \mathcal{H} / f^2$  is the propagation velocity of the Rossby waves,  $w_e = -\partial_y(\tau/\rho f)$  is the Ekman pumping, and  $\Delta h$  is the Laplacian of  $h$ . Terms in  $\epsilon^2$ ,  $\epsilon^3$ , ... have been neglected as the friction is small.

To obtain an analytical solution to Eq. (4), we assume that  $h$  varies in the meridional direction over spatial scales much larger than in the zonal direction, thus neglecting the derivative in  $y$ . This simplification is severe but comparable with that made in Frankignoul et al. (1997) and Sirven et al. (2002). Because of the coastal Kelvin waves, the signal at the eastern side  $x = L$  depends on the signal at the western side  $x = 0$ . We simply represent this dependence by prescribing that  $h(L, y, t) = h(0, y, t)$ . With these simplifications, the latitude  $y$  appears as a simple parameter in Eq. (4), and the two-dimensional problem has been reduced to a one-dimensional one described by

$$\partial_t H - c \partial_x H = -\lambda H + v \partial_{xx} H + w_e + \mathcal{S} \quad (5)$$

in which  $H(x, t)$  denotes the thermocline depth anomaly  $h(x, y, t)$  at latitude  $y$ , with  $H(0, t) = H(L, t)$  ( $v$  is defined by  $v = g' \epsilon / f^2$ ). The time evolution of the “volume anomalies”  $\int_0^L H(x, t) \, dx$  is prescribed. For simplicity, we assume that it remains equal to 0. This constraint replaces the initial global constraint on the volume  $\iint h \, dx \, dy = 0$ . It is rather general, as it does not prevent introducing sources or sinks of volume.

This model is simple but contains most of the physical ingredients included in the models where a volume constraint is applied (e.g., Cessi and Louazel 2001). It also extends the model of Frankignoul et al. (1997) by taking into account the existence of the boundaries and the mass conservation in a closed basin.

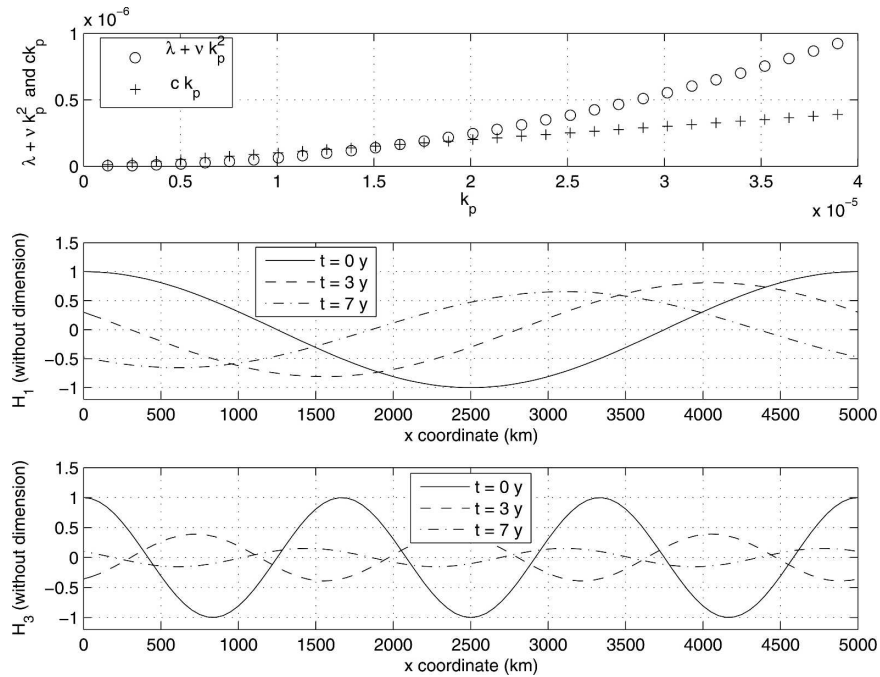


FIG. 1. Free modes in the one-dimensional model. (top) Eigenfrequencies  $ck_p$  and damping  $\lambda + \nu k_p^2$  in function of the eigenvalues  $k_p = 2p\pi/L$ . (middle) Least-damped eigenfunction  $H_1$  at  $t = 0, 3,$  and  $7$  yr. (bottom) Eigenfunction  $H_3$  at  $t = 0, 3,$  and  $7$  yr.

### b. Basin modes

As the model is defined in a finite domain, discrete basin modes are expected. These modes are defined from the operator  $\partial_t - c\partial_x + \lambda - \nu\partial_{xx}$ , including the boundary and mass conservation conditions; they therefore do not depend on the forcing fields. We thus search for these free modes by setting  $w_e + \mathcal{S} = 0$  and introducing  $H(x, t) = A \exp[i(\omega t + kx)]$  in Eq. (5). It yields  $\omega = ck + i(\lambda + \nu k^2)$  and  $H = A \exp[-(\lambda + \nu k^2)t] \exp[ik(x + ct)]$ . The boundary condition  $H(0, t) = H(L, t)$  leads to  $\exp(ikL) = 1$  so that  $k = 2p\pi/L$  with  $p$  positive integer. A discrete set of propagative damped free modes is thus found:

$$H_p(x, t) = a_p \exp[-(\lambda + \nu k_p^2)t] \cos[k_p(x + ct) + \phi_p], \quad (6)$$

with  $k_p = 2p\pi/L$ . Modes  $H_1$  and  $H_3$  are illustrated at different times in Fig. 1 for  $L = 5000$  km,  $c = 0.01$  m s $^{-1}$ ,  $\lambda^{-1} = 25$  yr, and  $\nu = 2.4 \times 10^6$  m $^2$  s $^{-1}$ . The free basin modes show an oscillating pattern whose amplitude does not depend on the zonal coordinate but decays exponentially with time. This pattern propagates westward with the Rossby wave celerity  $c$ . The mode  $H_1$  that has the largest wavelength and the lowest frequency is the least damped.

### c. Study of the forced response

When initial conditions are prescribed, an initial transient appears but is then damped because of the dissipation. As in Cessi and Otheguy (2003), we shall neglect this initial transient and focus on the forced response.

The model is forced by stochastic fluctuations in  $w_e + \mathcal{S}$ , which reflect changes in deep-water formation or wind stress. We consider the response to standing patterns because convection always occurs at about the same places (e.g., in the Labrador Sea) and the principal modes of low-frequency variability of the atmosphere in the midlatitude (e.g., the North Atlantic Oscillation) do not propagate. Our approach thus differs from that of Cessi and Otheguy (2003), who considered the more artificial case of a damped or a propagating forcing. This led them to introduce a complex angular frequency, whereas we shall consider a real angular frequency.

Observations indicate that the frequency spectrum of wind stress curl is nearly white at periods longer than 50 days (e.g., Mac Veigh et al. 1987). On the other hand, oceanic general circulation models suggest that the changes in the deep-water formation (represented by the anomalies of the mixed layer volume) have a slightly red spectrum at periods longer than a year (De-

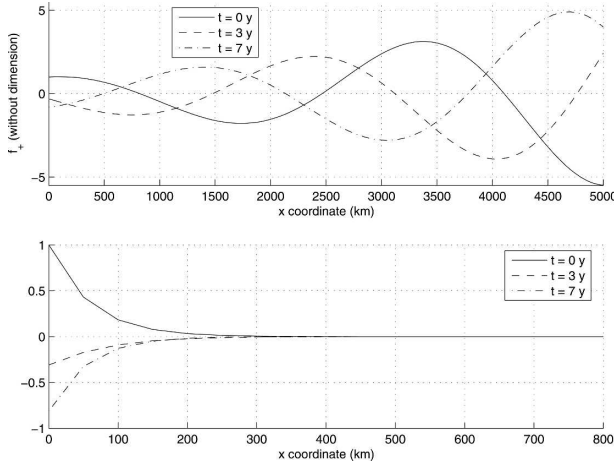


FIG. 2. Functions (top)  $f_+$  and (bottom)  $f_-$  times  $\exp(i\omega t)$  in the 1D model at  $t = 0, 3$ , and  $7$  yr. The pseudoperiod is equal to  $10$  yr (note the different scale in the bottom panel).

shayes and Frankignoul 2005). Nonetheless, for simplicity, we only consider here the case of a white noise forcing and assume that the Fourier transform of  $w_e + S$  does not depend on the angular frequency  $\omega$ ; hence, one has  $w_e + S = \Re[g(x)e^{i\omega t}]$  with  $\omega$  real. With these hypotheses, the forced response is of the form  $H = h_s(x) \exp(i\omega t)$ , where  $h_s$  is complex and obeys

$$h_s'' + 2\alpha_0 h_s' + \beta_0 h_s = G \tag{7}$$

with  $2\alpha_0 = c/v$ ,  $\beta_0 = (-\lambda - i\omega)/v$ , and  $G(x) = -g(x)/v$ .

The solutions of the homogeneous equation associated with Eq. (7) (hereinafter “free solutions”) differ from the free basin modes since the conditions  $H(t, 0) = H(t, L)$  and  $\int_0^L H(x, t) dx = 0$  do not apply (they apply to the complete solution). The characteristic equation reads  $r^2 + 2\alpha_0 r + \beta_0 = 0$ ; it admits two distinct roots:  $r_+ = -\alpha_0 + \Delta$  and  $r_- = -\alpha_0 - \Delta$  with  $\Delta^2 = \alpha_0^2 - \beta_0 = c^2/(4v^2) + (\lambda + i\omega)/v$ . To facilitate the discussion, we set  $\Delta = \rho e^{i\phi}$  with

$$\rho^2 = \frac{\sqrt{(c^2 + 4\lambda v)^2 + (4v\omega)^2}}{4v^2}$$

and

$$\tan 2\phi = \frac{4v\omega}{c^2 + 4\lambda v}$$

( $\rho > 0$  and  $2\phi \in [0, \pi/2]$ ) and write  $r_+ = d_+ + ik$  and  $r_- = d_- - ik$ , with  $d_+ = -\alpha_0 + \rho \cos\phi$ ,  $d_- = -\alpha_0 - \rho \cos\phi$ , and  $k = \rho \sin\phi$ . The free solutions are a linear combination of the functions  $f_+ = \exp(d_+ x) \exp(ikx)$  and  $f_- = \exp(d_- x) \exp(-ikx)$ .

The real part of  $f_+$  and  $f_-$  times  $\exp(i\omega t)$  are shown for different times in Fig. 2 for  $2\pi\omega^{-1} = 10$  yr. The

solution  $f_-$  (bottom panel) is a strongly damped signal that propagates eastward; it is thus negligible away from the western boundary. On the contrary,  $f_+$  (top panel) is a weakly damped signal that propagates westward. A simple computation shows that at low frequency, for  $\omega \ll \lambda + (c^2/4v)$ , the damping of  $f_+$  and  $f_-$  becomes nearly independent of the frequency. Moreover, the propagation velocity becomes equal to  $\pm\sqrt{c^2 + 4\lambda v}$ . Hence these solutions are very similar to free Rossby waves in a dissipative medium. Note that eastward propagation is tolerated because of the dissipative term: indeed, a balance between the Lagrangian derivative  $\partial_t - c\partial_x$  and the dissipative term  $v\Delta$  becomes possible for sufficiently short wavelengths.

The pattern associated with the free solution  $f_+$  (or  $f_-$ ) differs from the pattern of the free modes (e.g., the amplitude of  $f_+$  decays westward, whereas that of the basin modes remains constant). In Cessi and Otheguy (2003), the interior spatial structure is given by the function  $\exp[i\omega(x - L)/c]$ —which plays the same role as  $f_+$ —where  $\omega$  is complex and is given by the angular frequency of the forcing. When the imaginary part of  $\omega$  is positive, the amplitude of the pattern increases westward. The frequencies that are resonant verify this property, leading to patterns very similar to the basin modes. Here, because we consider the case of real angular frequency, the spatial pattern of  $f_+$  (which is characterized by the coefficients  $d_+$  and  $k$ ) always increases eastward since  $d_+$  is always positive. It thus does not resemble the free basin modes.

The solutions  $f_+$  and  $f_-$  do not verify the periodicity and volume conserving properties but are indispensable to write a solution of Eq. (7), which verifies them. Indeed, the latter can be written as  $h_s = c_+ f_+ + c_- f_-$  with the constraint  $0 = c'_+ f_+ + c'_- f_-$  (Lagrange’s method; the prime denotes the derivative of the functions  $c_+$  and  $c_-$ ). Introducing this constraint in Eq. (7), we find

$$c_+ = - \int_0^x \frac{G(X) dX}{(r_- - r_+) f_+(X)} + a_+ \quad \text{and}$$

$$c_- = \int_0^x \frac{G(X) dX}{(r_- - r_+) f_-(X)} + a_-$$

where  $a_-$  and  $a_+$  are two arbitrary constants [see Eq. (7) and the resolution that follows it for the definitions of  $G$ ,  $r_+$ , and  $r_-$ ]. This leads to

$$h_s = \frac{\mu(x)}{r_- - r_+} + a_+ f_+(x) + a_- f_-(x), \tag{8}$$

where

$$\mu(x) = -f_+(x) \int_0^x \frac{G(X) dX}{f_+(X)} + f_-(x) \int_0^x \frac{G(X) dX}{f_-(X)}.$$

The solution of Eq. (5) now reads  $H = h_s \exp(i\omega t)$ , where  $a_+$  and  $a_-$  are to be determined by the boundary condition and the mass constraint (we recall that the initial transient has been neglected).

The condition  $H(0, t) = H(L, t)$  gives

$$a_+ + a_- = \frac{\mu(L)}{r_- - r_+} + a_+ f_+(L) + a_- f_-(L). \quad (9)$$

Similarly, the condition  $\int_0^L H(x, t) dx = \int_0^L H_0(x) dx = 0$  gives

$$\int_0^L \left[ \frac{\mu(x)}{r_- - r_+} + a_+ f_+(x) + a_- f_-(x) \right] dx = 0. \quad (10)$$

These two relations lead to

$$a_+[1 - f_+(L)] = \frac{r_- r_+}{(r_+ - r_-)^2} \left[ \int_0^L \mu(x) dx - \frac{\mu(L)}{r_-} \right] \quad (11)$$

and

$$a_-[1 - f_-(L)] = \frac{r_- r_+}{(r_+ - r_-)^2} \left[ - \int_0^L \mu(x) dx + \frac{\mu(L)}{r_+} \right]. \quad (12)$$

Equations (8), (11), and (12) completely characterize the forced solution, which depends on three functions: the first one is  $\mu(x)$ , which mainly depends on the forcing  $G$ ; the second one is  $f_-$ , whose impact is limited to a narrow band near the western boundary; and the third one is  $f_+$ , which can influence the whole basin. The coefficient  $a_+$  depends on the details of the forcing and, in particular, its frequency. The module of  $a_+$  is maximal when  $\| [1 - f_+(L)](r_- - r_+)^2 \|$  is close to 0, that is, for sufficiently low frequency when  $\| [1 - f_+(L)] \|$  is minimal. As  $1 - f_+(L) = 1 - \exp(L\rho \cos\phi) \exp(iL\rho \sin\phi)$ , this leads to  $L\rho \sin\phi = 2p\pi$  and at low frequency to  $\omega/\sqrt{c^2 + 4\lambda\nu} = 2p\pi$ . The wavelength (frequency) is thus close to the wavelength (frequency) of the least-damped free mode, with a slight shift due to the dissipative processes (Fig. 3).

The decomposition in three wave terms of a forced solution has already been discussed by LaCasce (2000) (with a focus on the apparent phase speed of the waves) and in LaCasce and Pedlosky (2002) (with a focus on irregular basins). They used a quasigeostrophic model, where the conservation of mass induces a constraint on the streamfunction (its integral over the ocean basin is constant). They found free basin modes with complex frequencies, the imaginary part always differing from zero. When a forcing was applied (LaCasce and Pedlosky 2002, their section 4), they found that the response was maximal when the dispersion relation was minimal. In frequency space, the latter looks like a surface, with minima at the frequencies of the free basin

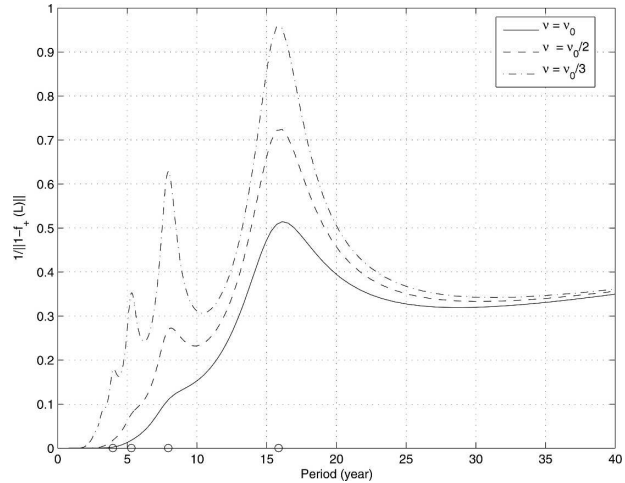


FIG. 3. Curves  $\|1 - f_+(L)\|^{-1}$  as a function of  $T = 2\pi/\omega$  for  $c = 0.01 \text{ m s}^{-1}$ ,  $\lambda^{-1} = 25 \text{ yr}$ , and  $\nu_0 = 600 \text{ m}^2 \text{ s}^{-1}$ . The periods corresponding to the four lowest frequencies of the basin modes [ $T = c/(pL)$ ,  $p = 1, 2, 3, 4$ ] are indicated by a circle on the abscissa.

modes. This surface, when it intersects the real frequency domain, has also maxima and minima (our Fig. 3 represents such a section, as it shows the amplitude of the free response). The minima have a real frequency close to the real frequency of the free basin modes (see their Fig. 1). In that sense, it can be said that the peaks in Fig. 3 are the traces in the real domain of the existence of basin modes in the complex domain. However, there is no reason to believe that the structure of the solution excited around these frequencies is similar to that of the free basin modes. On the contrary, our results suggest that it resembles the functions  $f_+$ , that is, damped long Rossby waves. Note that, when the viscosity vanishes, the function  $f_+$  becomes identical to the free basin modes for frequencies equal to the frequencies of the basin modes.

#### d. Influence of the spatial pattern of the forcing field

To complete this analysis, we investigate two contrasting situations: in the first one the forcing field is uniform  $G = G_0$ , while in the second one it is limited to a small area of the basin.

For  $G = G_0$  we have

$$\begin{aligned} \mu(x) &= G_0 \{ [1 - f_+(x)]/r_+ \} \\ &\quad - \{ [1 - f_-(x)]/r_- \}, \\ a_+[1 - f_+(L)] &= G_0 \frac{r_+ L + 1 - f_+(L)}{r_+(r_- - r_+)}, \quad \text{and} \\ a_-[1 - f_-(L)] &= G_0 \frac{r_- L + 1 - f_-(L)}{r_-(r_+ - r_-)}. \end{aligned}$$

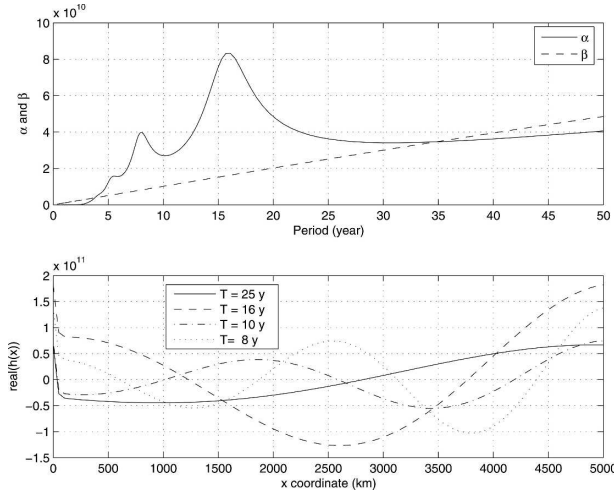


FIG. 4. (top) Values of  $L\|(r_- - r_+)[1 - f_+(L)]\|^{-1}$  and  $1/\|r_- r_+\|$  ( $c = 0.01 \text{ m s}^{-1}$ ,  $\lambda = 1/25 \text{ yr}^{-1}$ ,  $G_0 = 1$ , and  $\nu = 200 \text{ m}^2 \text{ s}^{-1}$ ) as a function of the period of the forcing. (bottom) Solution  $\Re[h_s(x)]$  for four different periods.

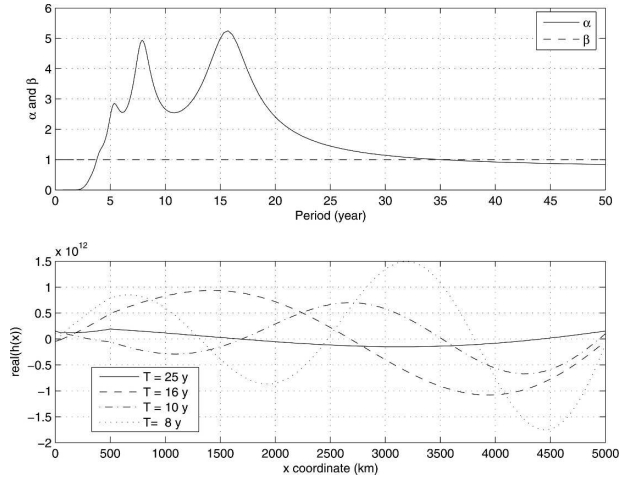


FIG. 5. (top) Values of  $\|(Lr_- - 1)r_+ / \{(r_- - r_+)[1 - f_+(L)]\}$  and  $\beta = 1$  ( $c = 0.01 \text{ m s}^{-1}$ ,  $\lambda = 1/25 \text{ yr}^{-1}$ ,  $G_0 = 1$ , and  $\nu = 200 \text{ m}^2 \text{ s}^{-1}$ ) as a function of the period of the forcing. (bottom) Solution  $\Re[h_s(x)]$  for four different periods.

And, consequently,

$$h_s(x) = G_0 \left\{ \frac{Lf_+(x)}{(r_- - r_+)[1 - f_+(L)]} - \frac{Lf_-(x)}{(r_- - r_+)[1 - f_-(L)]} + \frac{1}{r_- r_+} \right\}.$$

In the interior basin, the solution is dominated by the uniform forced term  $G_0/(r_- r_+)$  superposed to the propagative pattern  $f_+$ . The respective role of each term is illustrated in Fig. 4 (top), which shows the modulus of the coefficients  $\alpha = L/\{(r_- - r_+)[1 - f_+(L)]\}$  and  $\beta = 1/(r_- r_+)$  as a function of the period  $T = 2\pi/\omega$  of the forcing (these coefficients differ from  $a_+$  and  $\mu$  because of the nature of the forcing field:  $\alpha$  includes a part of the forced solution  $\mu$ ). Though  $\alpha$  differs from  $a_+$ , the curve representing  $\|\alpha\|$  in Fig. 4 (top) is very similar to the dash-dotted curve in Fig. 3, with a large peak close to the frequency of the least damped mode. However, the constant forcing term becomes dominant at very low frequency. Note that the power spectrum of the model response to a stochastic forcing with a white spectrum would be very comparable with the curve representing  $\|\alpha\|^2(\omega)$  in the frequency range where  $\beta$  is negligible (between 5 and 30 yr). Figure 4 (bottom) shows the function  $\Re[h_s(x)]$  for four forcing periods ( $T = 25, 16, 10,$  and  $8$  yr). As expected, the solution with the largest amplitude is that corresponding to  $T = 16$  yr, that is, the period for which  $\|\alpha\|$  exhibits the largest peak.

When the forcing is only applied on a small part of

the basin ( $G = G_0$  for  $0 \leq x \leq \epsilon$  with  $\epsilon \ll L$  and  $G = 0$  elsewhere), Eqs. (8), (11), and (12) become

$$\mu(x) = \begin{cases} G_0(r_- - r_+)x^2/2 & \text{if } x \leq \epsilon \\ G_0(r_- - r_+)\epsilon^2/2 & \text{if } x \geq \epsilon, \end{cases} \quad (13)$$

$$a_+[1 - f_+(L)] = \mu(\epsilon) \frac{(Lr_- - 1)r_+}{(r_- - r_+)^2}, \quad \text{and}$$

$$a_-[1 - f_-(L)] = \mu(\epsilon) \frac{(-Lr_+ + 1)r_-}{(r_- - r_+)^2},$$

where the high powers in  $\epsilon$  have been neglected. Last, one has

$$h_s(x) = \frac{G_0\epsilon^2}{2(r_- - r_+)} \left\{ \frac{(Lr_- - 1)r_+ f_+(x)}{[1 - f_+(L)]} + \frac{(-Lr_+ + 1)r_- f_-(x)}{[1 - f_-(L)]} + (r_- - r_+) \frac{x^2}{\epsilon^2} \right\}$$

if  $x \leq \epsilon$ . If  $x \geq \epsilon$ , the term  $x^2/\epsilon^2$  is replaced by 1.

The respective role of the forcing and the propagating terms is illustrated as before: Fig. 5 (top) shows the modulus of the coefficients  $\alpha = (Lr_- - 1)r_+ / \{(r_- - r_+)[1 - f_+(L)]\}$  and  $\beta = 1$  as a function of the period  $T$ . Two peaks of similar amplitude now occur in the  $\|\alpha\|$  curve. For a weaker dissipation coefficient (not shown), the peak at 8 yr becomes higher than the peak at 16 yr, indicating that the response would present higher frequencies and shorter wavelengths. Figure 5 (bottom) indicates that patterns with a wavelength of about 2500 km now have the largest amplitude.

These two examples illustrate that the free solutions

$f_+$ , which are very similar to long damped Rossby waves propagating westward in an open basin, allow conveniently to describe the part of the response that does not depend on the forcing. They also suggest that the spatial pattern of the forcing participates in selecting the dominant spatial and time scale of the response. When the forcing has a large spatial scale, resonance occurs at a period close to that of the least-damped basin mode. When the dissipation is weak and the forcing has a small spatial scale, the resonant period may be much shorter but still close to the period of a basin mode (e.g., the second mode).

### 3. Simulations with a numerical 1.5-layer model

#### a. Model description

The model is a shallow-water, reduced-gravity model with one active layer, whose mean thickness is 800 m, above an infinite layer at rest. It has been derived from a two-layer model described, for example, in Février et al. (2007). The model predicts the thickness  $h$  and the velocity  $\mathbf{v}$  of the active layer. The momentum conservation equation is

$$\frac{\partial \mathbf{v}}{\partial t} + (\text{curl} \mathbf{v} + f) \mathbf{k} \times \mathbf{v} = \nu \Delta_H \mathbf{v} - \text{grad}(g'h + \mathbf{v}^2/2), \quad (14)$$

where  $\nu$  is the turbulent viscosity coefficient and  $\mathbf{k}$  is a vector normal to the earth's surface. The reduced gravity  $g'$  is equal to  $0.008 \text{ m s}^{-2}$ . The mass conservation equation is

$$\frac{\partial h_1}{\partial t} + \text{div}(h_1 \mathbf{v}) = -\lambda h + S + w_e. \quad (15)$$

The basin extends from  $15^\circ$  to  $55^\circ\text{N}$ ,  $0^\circ$  to  $60^\circ\text{E}$ . The equations are solved by finite differences on a C grid on the sphere. The spatial resolution is equal to  $1/5^\circ$  and allows eddies to be represented by the model. The numerical scheme preserves enstrophy. No-slip boundary conditions are applied, and the gradient of  $h$  is assumed to vanish perpendicular to the boundary. The viscosity coefficient  $\nu$  is equal to  $100 \text{ m}^2 \text{ s}^{-1}$ . This model is very similar to that used by Huang et al. (2000), Cessi and Primeau (2001), or Primeau (2002). The results given below corresponds to the case  $\lambda = 0$ ; there is no significant change when  $\lambda^{-1} = 25 \text{ yr}$ , save that there is less energy at low frequency.

#### b. Basin modes of the 1.5-layer model

Eigenvalues and eigenmodes are searched by substituting the expressions  $h = \hat{h}(x, y)e^{\sigma t}$ ,  $u = \hat{u}(x, y)e^{\sigma t}$ , and  $v = \hat{v}(x, y)e^{\sigma t}$  into the linearized equations governing the 1.5-layer model. This leads to the system

$$\sigma \mathbf{v} = \mathbf{A} \mathbf{v}, \quad (16)$$

where

$$\mathbf{A} = \begin{pmatrix} 0 & -H\partial_x & -H\partial_y \\ -g'\partial_x & \nu\Delta & f \\ -g'\partial_y & -f & \nu\Delta \end{pmatrix} \quad \text{and} \quad \mathbf{v} = \begin{pmatrix} \hat{h} \\ \hat{u} \\ \hat{v} \end{pmatrix} \quad (17)$$

( $\sigma$  are the complex eigenvalues of the linear operator  $\mathbf{A}$ ). The resolution of this eigenvalue–eigenvector problem is done in spherical coordinates, the operator  $\mathbf{A}$  being discretized on a  $1^\circ \times 1^\circ$  grid using finite differences. The resolution has been degraded here in order to avoid numerical instabilities. The viscosity coefficient is correspondingly set to  $2500 \text{ m}^2 \text{ s}^{-1}$ . The technical computing software “Matlab” is used for this resolution.

The most weakly damped mode (Fig. 6, left) propagates westward and has a period of about 15 yr; its spatial pattern is very similar to that obtained by Cessi and Louazel (2001). It exhibits sequences of negative and positive lobes tilted southwestward, with maxima in the northwestern corner. The corresponding pattern of the meridional velocity  $\hat{v}$  is phase lagged with the pattern of  $\hat{h}$  in the interior basin and is more complex in the western boundary current. This is also found for the other modes that are weakly damped as illustrated in Fig. 6 (right). The characteristics of the modes are only changed by 1%–2% when a Newtonian drag  $\lambda \mathbf{v}$  (with  $\lambda = 10^{-7} \text{ s}^{-1}$ ) is added in the momentum equation. Similarly negligible variations are observed when the viscosity is reduced to  $1500 \text{ m}^2 \text{ s}^{-1}$  or when the resolution is increased by a factor of 2. Hence, the modes are robust and similar to those found by Cessi and Louazel (2001) on a  $\beta$  plane.

The amplitude of the basin modes in the 1.5-layer model increases northward and westward. For long waves, friction is weak in the basin interior and consequently does not significantly affect the pattern of the mode. On the contrary, the damping is mainly related to the boundary pressure adjustment when the wave interacts with the western boundary; the transmission of energy back to the eastern boundary is not complete since the wave fronts are not parallel to the boundary (Primeau 2002). To satisfy this constraint, the spatial pattern of the mode must be such that its amplitude increases westward. The northward amplification can be explained by the fact that the wave speed is smaller in the northern part of the basin. Hence, the waves are more damped northward; in order that the basin modes have a uniform decay rate everywhere in the basin, their amplitude must thus be stronger in its northern part. In other words, the spatial pattern of the mode can

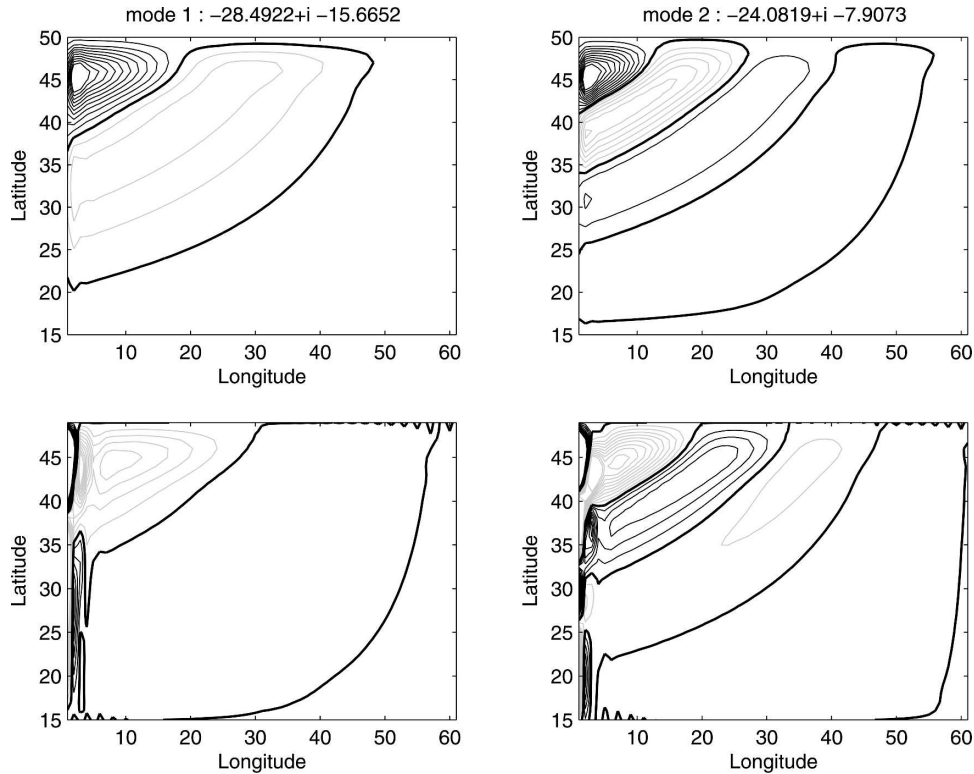


FIG. 6. First two least-damped eigenmodes of the 1.5-layer model. (top) First layer depth  $\hat{h}$  (m); (bottom) meridional velocity  $\hat{v}$  ( $\text{m s}^{-1}$ ).

largely be understood in terms of free waves and dissipation along the western boundary.

Note that we have not taken into account in the one-dimensional model the incomplete transmission of energy from the western boundary to the eastern one (Primeau 2002). It would be possible to account for it by assuming  $k > 1$  in the relation  $H(0, t) = kH(L, t)$ . A westward increase of the amplitude of the basin mode would be then observed in the one-dimensional model.

### c. Model response to stochastic forcing

Here we consider the response of the model to a mass forcing (e.g., induced by Ekman pumping). In the two experiments presented below, the forcings are the product of a spatial function  $F_i$  times a time function  $f(t)$ . The latter, which is the same for both experiments, is a random process with zero mean and a white spectrum.

In experiment E1, the forcing pattern is zonally independent and is given by  $F_1 = W_0 \sin(2\pi y/l)$  with  $W_0 = 10^{-6} \text{ m s}^{-1}$ . This pattern is similar to one used by Cessi and Louazel (2001). To illustrate the spatial pattern of the response, the first two EOFs of the meridional velocity, which together represent around 16% of

the total variance, are shown in Fig. 7. The associated principal components (PCs) are strongly correlated, indicating the westward propagation of the pattern. The autocorrelations of the PCs suggest the existence of an oscillation with a 13-yr period (Fig. 7d) close to the period of the least-damped basin mode. This time scale also emerges from the power spectrum of  $h$  north of  $30^\circ\text{N}$  and along the eastern side, as illustrated on Fig. 8 where a peak around 12–15 yr clearly appears [however, south of  $30^\circ\text{N}$ , the peak vanishes into a broad range of low-frequency variability and red spectra are obtained (not shown)]. The pattern displayed by the EOFs does not look like the least-damped basin mode shown in Fig. 6. Moreover, the regression of the meridional velocity onto the two PCs shows that the meridional velocity is damped while propagating westward (not shown).

In experiment E2, the function  $F_2$  is limited to the eastern part of the basin (between  $59^\circ$  and  $60^\circ\text{E}$ ) and latitude independent in order to compare two contrasting situations: the response to a weak injection of mass over a large geographical area (expt E1) and the response to a stronger and more localized mass injection (expt E2). In experiment E2, the EOF analysis also

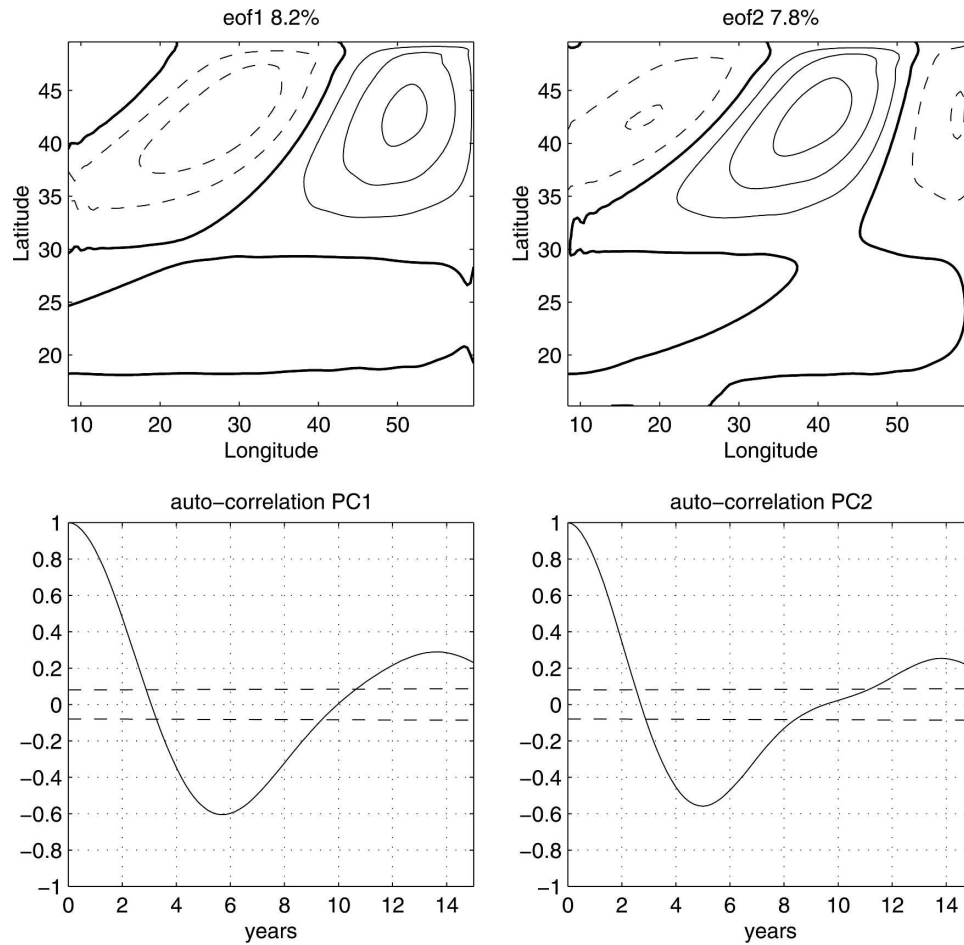


FIG. 7. First two EOFs of the meridional velocity and autocorrelation of the PCs in expt E1. The contour interval is  $0.2 \text{ mm s}^{-1}$  for the EOFs.

reveals the existence of a westward propagating oscillation, but the period is now about 1 yr, the spatial pattern is much shorter, and the maximum amplitude is located in the eastern half of the basin (Fig. 9).

These results show that oscillations, which are not

basin modes, can be excited by a stochastic injection of mass in a 1.5-layer model (for their links with basin modes, see the end of section 2c). The pattern associated with the dominant response differs from that of free basin modes whose maximum amplitude is found

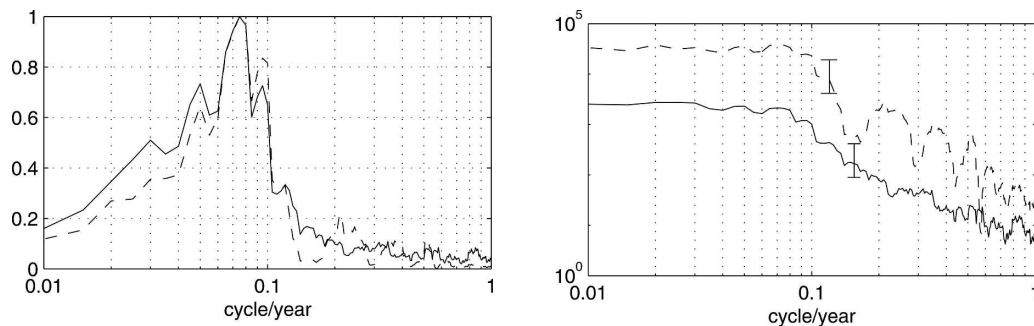


FIG. 8. Power spectrum of  $h$  in the midbasin, at  $40^\circ\text{N}$  (dashed line) and along the eastern side where it does not depend on the latitude (continuous line). (left) Each spectrum is divided by its maximum value and the representation is variance conserving; (right) the 95% confidence intervals.

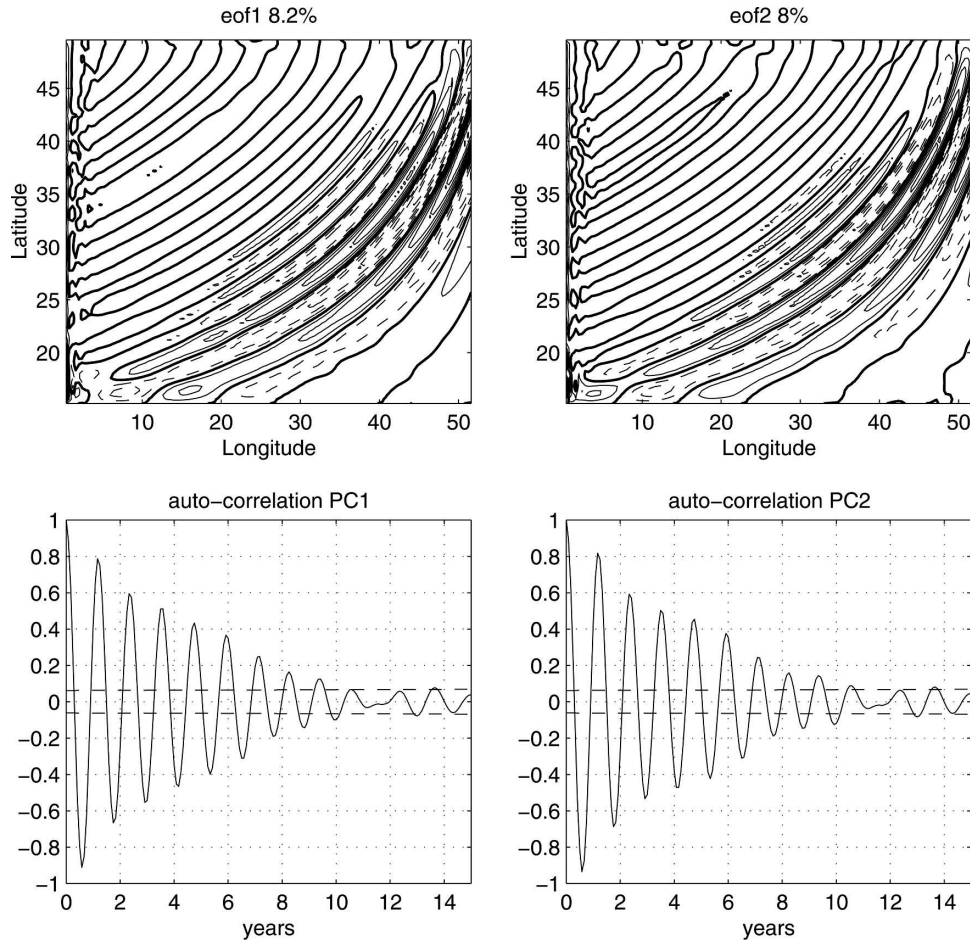


FIG. 9. As in Fig. 7 but for expt E2.

in the northwestern part of the basin. The present oscillations dwindle as they propagate westward, resembling damped propagating long Rossby waves excited at the eastern boundary. Also, the period of the dominant response is at decadal time scale for forcing with large zonal extent but may be at annual time scale if the zonal extent is small.

#### 4. Discussion and conclusions

A one-dimensional closed model of a midlatitude ocean basin has been developed in order to understand what determines the time scales of the ocean response to standing forcing. The model is of finite extension, satisfies the constraint of mass conservation, and represents the westward propagation of long Rossby waves across the basin. In this sense, it fills the gap between the simple model of Frankignoul et al. (1997) and the more complex one of Cessi and Louazel (2001) and Cessi and Otheguy (2003).

The analytical study of the response of this model to a prescribed harmonic forcing shows that part of the response does not depend on the spatial pattern of the forcing field. It consists of two propagative functions  $f_- \exp(i\omega t)$  and  $f_+ \exp(i\omega t)$ . The first one propagates eastward and is quickly damped so that it acts only near the western boundary. The second one has an oscillating spatial pattern that decays westward, the spatial scale of the decay being comparable to the zonal extent of the basin at low frequency. It propagates westward and behaves like a free long Rossby wave. The patterns of these functions differ from those of the free basin modes. The amplitude associated to the free solution  $f_+$  is largest when the frequency of the forcing is close to the frequencies of the free basin modes (a slight shift is observed because of friction). As explained in section 2c, this phenomenon occurs because the isolated minima of the dispersion relation in the complex frequency plane, which allows one to define the basin mode, are connected to the relative minima of the dis-

persion relation over the real frequency axis. Note that the physics that selects the frequency of the spectral peaks in the stochastically forced problem are basically the same as the physics that selects the weakly damped long-wave basin mode: the pressure perturbation along the eastern and western boundaries adjusts in order to produce constructive interferences. In addition to the free solutions, there is a forced one whose nature cannot be discussed independently of the spatial pattern of the forcing. In all cases, the zonal extent of the forcing influences the dominant time scale of the response, a more localized forcing favoring a shorter period.

Because of the obvious limitations of the analytical model, we have also examined the basin modes and analyzed the response to Ekman pumping or mass sources in a nonlinear numerical 1.5-layer model. In this model, the least-damped basin modes propagate westward, have maxima in the northwestern part of the basin, and have an annual to decadal period. The response of the model to large-scale forcing exhibits oscillations with period close to the periods of the least-damped basin modes. However, the patterns associated with these oscillations clearly differ from the basin modes: they peak off the eastern side and are damped as they propagate westward, thus resembling damped long Rossby waves. The spatial extent of the forcing influences the model response: the period of the dominant EOF is shorter if the forcing is more localized.

In the “open” model introduced by Frankignoul et al. (1997), the baroclinic response of the ocean at each frequency consists of a forced response plus a Rossby wave generated at the eastern boundary. The system adjusts so that there are no variations of the thermocline depth on the eastern boundary (a consequence of this setup is to produce doubled phase speed; Frankignoul et al. 1997; La Casce 2000). In the one-dimensional model developed here, the response consists of a forced response plus two functions that satisfy two constraints (mass conservation and energy transfer from the western to the eastern boundary because of coastal Kelvin waves). One of these functions ( $f_+$ ) has the spatial characteristics of a long damped Rossby wave and thus parallels the continuum of long Rossby waves of Frankignoul et al. (1997). However, we get resonances here because of the western wall; moreover, the power spectrum no longer vanishes near the eastern boundary.

Our results suggest that the variability of the ocean, when forced by standing stochastic patterns, is largely determined by the damped long Rossby waves. With this in mind, the problem is more usefully thought of in terms of these free waves. In particular, one better un-

derstands why one-dimensional models with no western boundary broadly succeed in reproducing the spectral characteristics of the ocean at annual to decadal time scales far from the eastern boundary (Sirven et al. 2002; Baquero-Bernal and Latif 2005). Indeed, because of the complexity of the conditions in a real ocean (the western boundary is not a wall, the forcing does not have a simple spatial pattern, etc.), resonant peaks are damped and a smoother spectrum must appear, generated by the westward propagation of the long Rossby waves.

*Acknowledgments.* We thank the reviewers for their comments, which were helpful in improving the manuscript. This work is supported by the EU Framework 6 programme under contract 003903-GOCE (DYNAMITE). Computations have been done at the Institut du Développement et des Ressources en Informatique Scientifique.

#### REFERENCES

- Baquero-Bernal, A., and M. Latif, 2005: Wind-driven oceanic Rossby waves in the tropical south Indian Ocean with and without an active ENSO. *J. Phys. Oceanogr.*, **35**, 729–746.
- Cessi, P., and S. Louazel, 2001: Decadal oceanic response to stochastic wind forcing. *J. Phys. Oceanogr.*, **31**, 3020–3029.
- , and F. Primeau, 2001: Dissipative selection of low-frequency modes in a reduced-gravity basin. *J. Phys. Oceanogr.*, **31**, 127–137.
- , and P. Otheguy, 2003: Oceanic teleconnections: Remote response to decadal wind forcing. *J. Phys. Oceanogr.*, **33**, 1604–1617.
- Deser, C., M. A. Alexander, and M. A. Timlin, 1999: Evidence for a wind-driven intensification of the Kuroshio Current Extension from the 1970s to the 1980s. *J. Climate*, **12**, 1697–1706.
- Deshayes, J., and C. Frankignoul, 2005: Spectral characteristics of the response of the meridional overturning circulation to deep-water formation. *J. Phys. Oceanogr.*, **35**, 1813–1825.
- Février, S., J. Sirven, and C. Herbaut, 2007: Interaction of a coastal Kelvin wave with the mean state in the Gulf Stream separation area. *J. Phys. Oceanogr.*, **37**, 1429–1444.
- Frankignoul, C., P. Müller, and E. Zorita, 1997: A simple model of the decadal response of the ocean to stochastic wind stress forcing. *J. Phys. Oceanogr.*, **27**, 1533–1546.
- Huang, R. X., M. A. Cane, N. Naik, and P. Goodmand, 2000: Global adjustment of the thermocline in response to deep water formation. *Geophys. Res. Lett.*, **27**, 759–762.
- Johnson, H. L., and D. P. Marshall, 2002: A theory for the surface Atlantic response to thermohaline variability. *J. Phys. Oceanogr.*, **32**, 1121–1132.
- , and —, 2004: Global teleconnections of meridional overturning circulation anomalies. *J. Phys. Oceanogr.*, **34**, 1702–1722.
- Kushnir, Y., 1994: Interdecadal variations in North Atlantic sea surface temperature and associated atmospheric conditions. *J. Climate*, **7**, 141–157.
- LaCasce, J. H., 2000: Baroclinic Rossby waves in a square basin. *J. Phys. Oceanogr.*, **30**, 3161–3178.

- , and J. Pedlosky, 2002: Baroclinic Rossby waves in irregular basins. *J. Phys. Oceanogr.*, **32**, 2828–2847.
- , and —, 2004: The instability of Rossby basin modes and the oceanic eddy field. *J. Phys. Oceanogr.*, **34**, 2027–2041.
- Mac Veigh, J. P., B. Barnier, and C. Le Provost, 1987: Spectral and empirical orthogonal functions analysis of four years of European Center for Medium Range Weather Forecast wind stress curl over the North Atlantic Ocean. *J. Geophys. Res.*, **92**, 13 141–13 152.
- Milliff, R. F., and J. C. McWilliams, 1994: The evolution of boundary pressure in ocean basins. *J. Phys. Oceanogr.*, **24**, 1317–1338.
- Primeau, F., 2002: Long Rossby wave basin-crossing time and the resonance of low-frequency basin modes. *J. Phys. Oceanogr.*, **32**, 2652–2665.
- Sirven, J., C. Frankignoul, G. de Coëtlogon, and V. Taillandier, 2002: Spectrum of wind-driven baroclinic fluctuations of the ocean in the midlatitudes. *J. Phys. Oceanogr.*, **32**, 2405–2417.
- Wajsowicz, R. C., and A. E. Gill, 1986: Adjustment of the ocean under buoyancy forces. Part I: The role of Kelvin waves. *J. Phys. Oceanogr.*, **16**, 2097–2114.